

# $N_{\text{H}}$ - $N_{\text{HI}}$ correlation in Gigahertz-peaked-spectrum galaxies \*

L. Ostorero<sup>1,2,\*\*</sup>, R. Morganti<sup>3,4</sup>, A. Diaferio<sup>1,2</sup>, A. Siemiginowska<sup>5</sup>, Ł. Stawarz<sup>6</sup>, R. Moderski<sup>7</sup>, and A. Labiano<sup>8</sup>

<sup>1</sup> Dipartimento di Fisica, Università degli Studi di Torino, Via P. Giuria 1, 10125 Torino, Italy

<sup>2</sup> Istituto Nazionale di Fisica Nucleare (INFN), Via P. Giuria 1, 10125 Torino, Italy

<sup>3</sup> Netherlands Institute for Radio Astronomy, Postbus 2, 7990 AA Dwingeloo, The Netherlands

<sup>4</sup> Kapteyn Astronomical Institute, University of Groningen, P.O. Box 800, 9700 AV Groningen, The Netherlands

<sup>5</sup> Harvard-Smithsonian Center for Astrophysics, 60 Garden St., Cambridge, MA 02138, USA

<sup>6</sup> Astronomical Observatory, Jagiellonian University, ul. Orla 171, 30-244 Kraków, Poland

<sup>7</sup> Nicolaus Copernicus Astronomical Center, Bartycka 18, 00-716 Warsaw, Poland

<sup>8</sup> Institute for Astronomy, Department of Physics, ETH Zurich, CH-8093 Zurich, Switzerland

Received XXXX, accepted XXXX

Published online XXXX

**Key words** galaxies: active, galaxies: ISM, ISM: clouds, radio lines: galaxies, X-rays: galaxies

With the Westerbork Synthesis Radio Telescope, we performed HI observations of a sample of known X-ray emitting Gigahertz-peaked-spectrum galaxies with compact-symmetric-object morphology (GPS/CSOs) that lacked an HI absorption detection. We combined radio and X-ray data of the full sample of X-ray emitting GPS/CSOs and found a significant, positive correlation between the column densities of the total and neutral hydrogen ( $N_{\text{H}}$  and  $N_{\text{HI}}$ , respectively). Using a Bayesian approach, we simultaneously quantified the parameters of the  $N_{\text{H}}$  -  $N_{\text{HI}}$  relation and the intrinsic spread of the data set. For a specific subset of our sample, we found  $N_{\text{H}} \propto N_{\text{HI}}^b$ , with  $b = 0.93^{+0.49}_{-0.33}$ , and  $\sigma_{\text{int}}(N_{\text{H}}) = 1.27^{+1.30}_{-0.40}$ . The  $N_{\text{H}}$  -  $N_{\text{HI}}$  correlation suggests a connection between the physical properties of the radio and X-ray absorbing gas.

Copyright line will be provided by the publisher

## 1 Introduction

Compact radio galaxies with GHz-peaked spectrum (GPS) and compact-symmetric-object (CSO) morphology, hereafter referred to as GPS/CSOs, are powerful, sub-kiloparsec scale sources that likely represent the youngest fraction of the radio galaxy population (e.g., O’Dea 1998; Orienti 2015). Their radio emission is dominated by the mini-lobes, fully contained in the host galaxy interstellar medium. Although they are increasingly detected in the X-ray domain (O’Dea et al. 2000; Risaliti et al. 2003; Guainazzi et al. 2004, 2006; Vink et al. 2006; Siemiginowska et al. 2008; Tengstrand et al. 2009), the best angular resolution currently available ( $\sim 1''$  with *Chandra*) is not sufficient to resolve the X-ray morphology of most GPS/CSOs. Therefore, the origin of their X-ray emission is still matter of debate (e.g., Siemiginowska et al. 2009; Migliori 2015).

Both the radio and the X-ray emission display significant absorption. However, the location of the radio and X-ray absorbers in the host galaxy of the radio source are still debated too. In the limited sample of compact sources with available high angular resolution HI absorption measurements, the HI is typically detected against one or both radio lobes (Araya et al. 2010, and references therein; Morganti et al. 2013), with estimated covering factors,  $C_{\text{f}}$ , vari-

able from  $\sim 0.2$  to  $\sim 1$  (e.g., Peck et al. 1999; Morganti et al. 2004). The general consensus is that the HI absorber has an inhomogeneous or clumpy nature, although the actual distribution of the gas is not known.

Hard X-ray (2–10 keV) spectra of GPS/CSOs reveal a mean value of the column density much higher than that of a control sample of extended radio galaxies of the FR-I type (whose core emission appears to be generally unobscured by an optically thick torus), and intermediate between the values of unobscured and highly obscured FR-II radio galaxies, where the presence of an optically thick torus is supported by optical and X-ray observations (Tengstrand et al. 2009, and references therein). Any relationship between the radio and X-ray absorbers may thus help to clarify the absorption picture.

A comparison between  $N_{\text{H}}$  and  $N_{\text{HI}}$  for a sample of GPS/CSOs showed that the  $N_{\text{H}}$  values are systematically higher than the  $N_{\text{HI}}$  values of 1–2 orders of magnitudes (Vink et al. 2006; Tengstrand et al. 2009). Because the estimate of  $N_{\text{HI}}$  depends on the ratio between the spin temperature of the absorbing gas and its source covering factor,  $T_{\text{s}}/C_{\text{f}}$  (see Equation 2), the magnitude of this offset can change according to the  $T_{\text{s}}/C_{\text{f}}$  parameter, which is poorly constrained (Ostorero et al. 2010, and references therein; Curran et al. 2013). Regardless of its magnitude, however, the existence of a systematic offset might in itself indicate a connection between

\* Data from the Westerbork Synthesis Radio Telescope

\*\* Corresponding author: e-mail: ostorero@ph.unito.it

**Table 1** GPS/CSO sources of our sample: source names, optical redshifts, type of  $N_{\text{HI}}$  data (from spatially unresolved measurements) and of  $N_{\text{H}}$  data included in the present analysis (V: value, UL: upper limit, NA: not available because of bad data quality, IP: analysis in progress) and corresponding references (\*: this work, and Ostorero et al., in prep.; \*\*: Siemiginowska et al., in prep.; numbers refer to papers cited in the reference list, where they are included in square brackets).

Source name (B1950)	$z_{\text{opt}}$	$N_{\text{HI}}$	Ref.	$N_{\text{H}}$	Ref.
0026+346	0.517	NA	*	V	9
0108+388	0.66847	V	1	LL	10
0116+319	0.06	V	2	IP	**
0428+205	0.219	V	3	UL	10
0500+019	0.58457	V	4	V	10
0710+439	0.518	NA	*	V	10
0941-080	0.228	V	*	UL	11,12
1031+567	0.450	V	*	V	10
1117+146	0.362	UL	*	UL	10
1323+321	0.370	V	3	V	10
1345+125	0.12174	V	5	V	10,12
1358+624	0.431	V	3	V	10
1404+286	0.07658	V	1	V	13
1607+268	0.473	UL	*	UL	10
1843+356	0.764	UL	*	IP	**
1934-638	0.18129	V	6	UL	14
1946+708	0.101	V	7,8	V	14
2008-068	0.547	NA	*	UL	10
2021+614	0.227	UL	*	IP	**
2128+048	0.99	UL	*	V,UL	9,10
2352+495	0.2379	V	3	V	10

X-ray and radio absorbers, and deserves to be investigated statistically.

In a sample of 10 GPS/CSOs, whose  $N_{\text{H}}$  and  $N_{\text{HI}}$  measurements were available in the literature, we discovered a significant, positive  $N_{\text{H}}-N_{\text{HI}}$  correlation (Ostorero et al. 2009, 2010), with  $N_{\text{H}}$  and  $N_{\text{HI}}$  linked through the relationship  $N_{\text{H}} \propto N_{\text{HI}}^b$ , with  $b \simeq 1$ . With the aim of improving the statistics of the  $N_{\text{H}}-N_{\text{HI}}$  correlation sample, we carried out a program of observations of the known X-ray emitting GPS/CSOs lacking an HI absorption detection with the Westerbork Synthesis Radio Telescope (WSRT). In this paper, we report the first results of this project.

## 2 Source sample

We studied the HI and X-ray absorption properties of the full sample of GPS galaxies known as X-ray emitters to date. This sample is composed of 21 sources, belonging to at least one of the following GPS samples: Stanghellini et al. (1998), Snellen et al. (1998), Tornaiainen et al. (2007), and Vermeulen et al. (2003). All of these sources were also classified as CSOs. The source list is given in Table 1.

## 3 HI observations with the WSRT

With the WSRT, we searched for HI absorption the 10 sources of our sample (marked with a star in Column 4 of Table 1) that still lacked an HI detection, either because they were never observed or because previous observations yielded only upper limits to the HI optical depth.

Each target was observed for an exposure time of four to 12 hours with the UHF-high-band receiver (appropriate when  $z \gtrsim 0.2$ ) in dual orthogonal polarisation mode. The observing band was 10 to 20 MHz wide, with 1024 spectral channels, and was centered at the frequency where the HI absorption line is expected to occur based on the optical redshift. Compared to the HI survey of compact sources by Vermeulen et al. (2003), our observations could benefit from a larger ratio between number of spectral channels and observing band width: this improvement, together with the longer exposure times, enabled a more effective separation of narrow HI absorption features from radio frequency interferences (RFI) in most of the previously observed sources. The data reduction process and the results of the analysis will be presented elsewhere.

We detected HI absorption in two out of 10 targets. For five targets, we could estimate upper limits to the line optical depth and to the HI column density. For three of our targets, RFI were too strong to obtain any useful data (see Table 1).

The atomic hydrogen column density along the line of sight is related to the velocity integrated optical depth of the 21-cm absorption via the following relationship (Wolfe & Burbidge 1975):

$$N_{\text{HI}} = 1.823 \times 10^{18} T_s \int \tau dv. \quad (1)$$

In the optically thin regime (i.e. for  $\tau \lesssim 0.3$ ), Equation 1 is approximated by

$$N_{\text{HI}} \approx 1.823 \times 10^{18} (T_s/C_f) \int \tau_{\text{obs}} dv, \quad (2)$$

where  $\tau_{\text{obs}} \equiv \Delta S/S$  is the observed optical depth of the line, given by the ratio between the spectral line depth ( $\Delta S$ ) and the continuum flux ( $S$ ) of the background radio source, and is related to the actual optical depth through  $\tau \approx \tau_{\text{obs}}/C_f$ . For homogeneity with literature data, we estimated the HI column densities by assuming that the absorber fully covers the radio source ( $C_f=1$ ) and that the spin temperature is  $T_s=100$  K. These assumptions yielded  $N_{\text{HI}}$  values that are lower limits to the actual column densities. When no HI line was detected, upper limits to  $N_{\text{HI}}$  were estimated from the optical depth upper limits ( $\tau_{3\sigma}$ ) that we derived from the 3- $\sigma$  noise level.

## 4 $N_{\text{H}}-N_{\text{HI}}$ correlation

We investigated the existence of a correlation between the neutral hydrogen column density ( $N_{\text{HI}}$ ) and the total hydrogen column density ( $N_{\text{H}}$ ), with the aim of either confirming or disproving the significant, positive  $N_{\text{H}}-N_{\text{HI}}$  correlation

that we discovered for a smaller sample of 10 GPS/CSOs (Ostorero et al. 2009, 2010). Below, we describe the selection of the correlation sample and present the first results of the correlation analysis.

#### 4.1 $N_{\text{HI}}$ sample

HI absorption detections and corresponding  $N_{\text{HI}}$  values were available for 13 out of 21 sources of the sample;  $N_{\text{HI}}$  upper limits could be estimated for five sources; for three sources, no useful data were obtained (see Table 1).

Because multiple spectral features were detected in the HI absorption spectra of a subsample of sources, different  $N_{\text{HI}}$  values could be associated to the same source. Here, we present the result of the analysis that we performed by taking the *total*  $N_{\text{HI}}$  of the detected absorption features into account. The full record of cases will be presented elsewhere. When more than one total  $N_{\text{HI}}$  estimate was available for a given source, we chose the most recent result from spatially unresolved measurements.

#### 4.2 $N_{\text{H}}$ sample

Estimates of the total hydrogen column densities ( $N_{\text{H}}$ ) were available for 18 out of 21 sources: 11 of them are  $N_{\text{H}}$  values, six of them are upper limits, and one of them is a lower limit to  $N_{\text{H}}$ . For the remaining sources, the analysis is in progress (see Table 1).

The  $N_{\text{H}}$  estimates were derived from the X-ray spectral analysis by fitting a model spectrum, absorbed by both a Galactic and a local (i.e., at redshift  $z_{\text{opt}}$ ) gas column density, to the observed X-ray spectrum; in the fitting procedure, the  $N_{\text{H}}$  parameter was left free to vary. For some sources, more than one model could be fit to the spectrum, yielding different  $N_{\text{H}}$  best-fit estimates. In particular, four sources (1404+286, 1607+268, 1934-638, and 1946+708) could satisfactorily be interpreted as both Compton-thin and Compton-thick X-ray sources: here, we present the analysis performed by taking the Compton-thin  $N_{\text{H}}$  values only into account; the full record of cases will be discussed elsewhere. Furthermore, for one source (0108+388), the available lower limit to  $N_{\text{H}}$  is consistent with both a Compton-thin and a Compton-thick scenario: again, here we present the results of the analysis performed under the assumption that the source is Compton-thin. For five sources of the sample, different  $N_{\text{H}}$  estimates were derived from observations carried out in different epochs. Because we cannot rule out long-term column-density variations, when different values were not consistent with each other at the  $1-\sigma$  level (as for 1345+125) and when both values and upper limits were available (as for 2128+048), we chose to include the two extreme  $N_{\text{H}}$  estimates in our correlation sample, each of them associated to the same  $N_{\text{HI}}$  value. Including either the average or any of the two  $N_{\text{H}}$  estimates does not change our results significantly.

#### 4.3 $N_{\text{H}} - N_{\text{HI}}$ sample

Pairs of  $N_{\text{HI}}$  and  $N_{\text{H}}$  values (V-V pairs in Table 1) were available for a subsample of eight sources, hereafter referred to as the *detection correlation sample*,  $D$ . We also define a second *detection correlation sample*,  $D'$ , which includes, besides the sources of sample  $D$ , source 0108+388, for which a proper detection is not available. Under the assumption that the source is Compton thin (see Section 4.2) an  $N_{\text{H}}$  value can be estimated as the mean of the  $3-\sigma$  lower limit and the physical upper bound of the Compton-thin  $N_{\text{H}}$  range (i.e.,  $N_{\text{H}} = 9.0 \times 10^{23} \text{ cm}^{-2}$ ). We consider the  $N_{\text{H}}$  range as a  $\pm 3\sigma$  interval, and thus associate to the mean  $N_{\text{H}}$  the corresponding  $1-\sigma$  error. Pairs of  $N_{\text{HI}}$  and  $N_{\text{H}}$  estimates (i.e., pairs including detections and/or upper limits: V-V, V-UL, UL-V, and UL-UL pairs in Table 1) were available for a subsample of 14 sources, hereafter referred to as the *estimate correlation sample*,  $E$ . As we did for the detections, we also define a second *estimate correlation sample*,  $E'$ , which includes sample  $E$  and source 0108+388.

#### 4.4 Correlation analysis

Figures 1 and 2 display the  $(N_{\text{HI}}, N_{\text{H}})$  data for the *detection* and *estimate correlation samples*, respectively.

First, we performed the correlation analysis on the *detection correlation sample*. A Pearson correlation analysis applied to sample  $D$  did not reveal a significant correlation. This result is confirmed by the more robust, *non-parametric* (or *rank*) methods, i.e. Spearman's and Kendall's correlation analysis (Press 1992). The main reason why we do not confirm the result found for the detections in our previous paper (Ostorero et al. 2009, 2010) is that we replaced the  $N_{\text{H}}$  values that were derived by fixing the X-ray spectral index (Vink et al. 2006) with more robust estimates (Tengstrand et al. 2009). We also chose to include source 1404+286 (with a complex X-ray spectrum) in our sample.

We then repeated the Pearson correlation analysis for sample  $D'$ , and we find a positive, significant correlation (correlation coefficient:  $r = 0.93$ ; probability of the null-hypothesis of no correlation being true:  $P = 7.8 \times 10^{-5}$ ). The statistical significance of this correlation, however, is admittedly driven by source 0108+388, characterized by the largest  $(N_{\text{HI}}, N_{\text{H}})$  values. Indeed, in the same sample, the evaluation of the correlation by means of the more robust Spearman's and Kendall's correlation analysis dramatically decreased the significance of the above result ( $P = 0.3$ ).

In the *estimate correlation sample*, we investigated the correlation by means of survival analysis techniques. In particular, we made use of the software package ASURV Rev. 1.3<sup>1</sup> (Lavalley, Isobe & Feigelson 1992), which implements the methods for bivariate problems presented in Isobe, Feigelson & Nelson (1986). The ASURV generalized Spearman's and Kendall's correlation analysis applied to sample  $E$  shows that the data are significantly correlated ( $P = 1.8 \times 10^{-2}$  –

<sup>1</sup> <http://www2.astro.psu.edu/statcodes/asurv/>

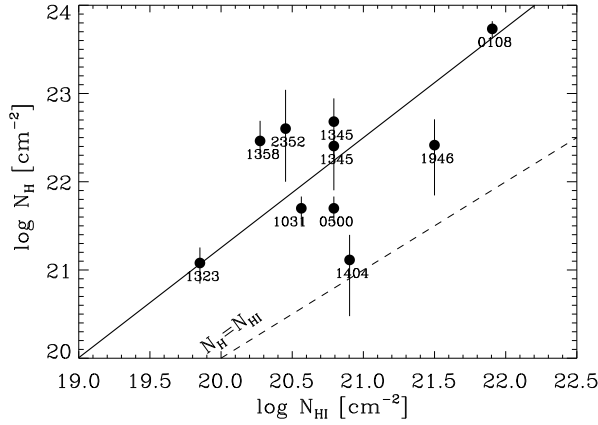


**Fig. 1** X-ray column densities ( $N_{\text{H}}$ ) as a function of radio column densities ( $N_{\text{HI}}$ ) for the  $D'_1$  sample. The solid symbols show the  $(N_{\text{HI}}, N_{\text{H}})$  measurements with  $1-\sigma$  error bars on  $N_{\text{H}}$ .  $N_{\text{HI}}$  was computed by assuming  $T_{\text{s}} = 100$  K and  $C_{\text{f}} = 1$ . Labels show a shortened version of the source names reported in Table 1. Solid line: linear regression best-fit line to the data (to guide the eye;  $\log N_{\text{H}} = a + b \log N_{\text{HI}}$ , with  $a = -3.68$  and  $b = 1.25$ ); dashed line: bisector of the  $N_{\text{HI}}-N_{\text{H}}$  plane. Data are from references listed in Table 1.

$3.8 \times 10^{-2}$ ). For sample  $E'$ , including source 0108+388<sup>2</sup> the significance improved further ( $P = 6.5 \times 10^{-3} - 9 \times 10^{-2}$ ).

As far as the law describing the relationship between  $N_{\text{H}}$  and  $N_{\text{HI}}$  is concerned, according to Pearson's test we could fit a linear relation to the *detection sample*  $D'$ :  $\log N_{\text{H}} = a + b \log N_{\text{HI}}$ , with  $a = -3.68 \pm 1.72$  and  $b = 1.25 \pm 0.08$ . However, this relation is not a good description of the data ( $\chi^2_{\text{red}} = 6.73$ ): the dispersion of the data is clearly larger than the typical uncertainties on  $N_{\text{H}}$  (see Figure 1).

As for the *estimate samples*,  $E$  and  $E'$ , the ASURV Schmitt's linear regression enabled us to perform a linear fit to the data (the estimated best-fit slope is  $b = 0.59$ ) but not to evaluate the goodness of the fit. A visual inspection of this data set again confirms a dispersion larger than the typical  $N_{\text{H}}$  uncertainties (see Figure 2). This fact suggests that additional variables are involved in the correlation, and the  $N_{\text{H}} - N_{\text{HI}}$  relation is the two-dimensional projection of a more complex relation.

#### 4.5 Bayesian analysis

In order to derive the correlation parameters of the  $N_{\text{H}} - N_{\text{HI}}$  relation and the intrinsic scatter of the data set, it is appropriate to resort to Bayesian analysis. Given our data set  $DS = \{x^i, y^i, S_1^i, S_2^i\}$ , where  $\{x^i\} = \{\log N_{\text{HI}}^i\}$  and  $\{y^i\} = \{\log N_{\text{H}}^i\}$  are the vectors of the  $\log N_{\text{HI}}$  and  $\log N_{\text{H}}$  values, respectively,  $\{S_1^i\}$  and  $\{S_2^i\}$  are the vectors of the

<sup>2</sup> for 0108+388, we still use the  $N_{\text{H}}$  value estimated as described in Section 4.2, instead of the lower limit, because ASURV cannot deal with two types of data censoring.

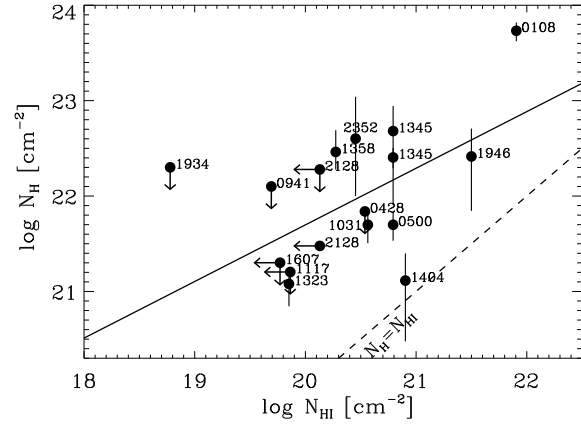


**Fig. 2** X-ray column densities ( $N_{\text{H}}$ ) as a function of radio column densities ( $N_{\text{HI}}$ ) for the  $E'_1$  sample. The solid symbols show the  $(N_{\text{HI}}, N_{\text{H}})$  measurements with  $1-\sigma$  error bars on  $N_{\text{H}}$ .  $N_{\text{HI}}$  was computed by assuming  $T_{\text{s}} = 100$  K and  $C_{\text{f}} = 1$ . Arrows represents upper limits. Labels show a shortened version of the source names reported in Table 1. Solid line: linear regression best-fit line to the data (to guide the eye;  $\log N_{\text{H}} = a + b \log N_{\text{HI}}$ , with  $a = -9.8$  and  $b = 0.59$ ); dashed line: bisector of the  $N_{\text{HI}}-N_{\text{H}}$  plane. Data are from references listed in Table 1.

upper and lower uncertainties on the  $\{y^i\}$  values, and  $i$  runs from 1 to the number of data points,  $N$ , we determined the multi-dimensional probability density function (PDF) of the parameters  $\theta = \{a, b, \sigma_{\text{int}}\}$ . Here,  $a$  and  $b$  are the parameters of the correlation:  $y = a + bx$ . In order to mimic additional hidden parameters in the relation, we assumed that  $y^i$  is a random variate with mean  $\bar{y}^i = a + bx^i$  and variance  $\sigma_{\text{int}}^2$ , with  $\sigma_{\text{int}}$  the intrinsic scatter of the dependent variable (e.g., Andreon & Hurn 2010).

For our Bayesian analysis, we used the code APEMoST<sup>3</sup>, developed by J. Buchner and M. Gruberbauer (e.g., Gruberbauer 2009). Because this code cannot deal with censored data, we restrict our Bayesian analysis to the *detection sample*  $D'$ . We assumed independent flat priors for parameters  $a$  and  $b$ , except for the internal dispersion  $\sigma_{\text{int}}$ , which is positive defined. We use  $2 \times 10^6$  MCMC iterations to guarantee a fairly complete sampling of the parameter space. The boundaries of the parameter space were set to  $[-1000, 1000]$  for the  $a$  and  $b$  parameters,  $[0.01, 1000]$  for the  $\sigma_{\text{int}}$  parameters. The initial seed of the random number generator was set with the bash command `GSL_RANDOM_SEED=$RANDOM`.

Our analysis shows that, for any given value of  $\log N_{\text{HI}}$ ,  $\log N_{\text{H}}$  takes the value  $\log N_{\text{H}} = a + b \log N_{\text{HI}} \pm \sigma_{\text{int}}$  (with  $a = 2.78^{+6.82}_{-9.83}$ ,  $b = 0.93^{+0.49}_{-0.33}$ , and  $\sigma_{\text{int}} = 1.27^{+1.30}_{-0.40}$ ) with a 68 percent probability. As an example, when  $N_{\text{HI}}$  is equal to  $10^{20} \text{ cm}^{-2}$ ,  $N_{\text{H}}$  varies in the interval  $(10^{20.11} - 10^{22.65})$ .

<sup>3</sup> Automated Parameter Estimation and Model Selection Toolkit; <http://apemost.sourceforge.net/>, Feb. 2011.



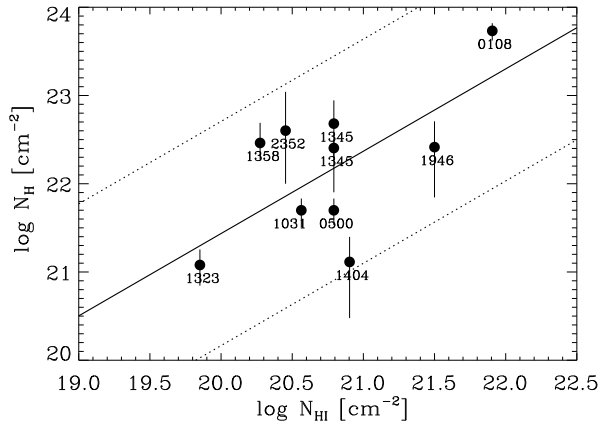


**Fig. 3** Bayesian analysis applied to sample  $D'_1$ . The solid symbols show the  $(N_{\text{HI}}, N_{\text{H}})$  measurements with  $1\text{-}\sigma$  error bars on  $N_{\text{H}}$ . The solid, straight-line is the  $N_{\text{H}} - N_{\text{HI}}$  relation:  $\log N_{\text{H}} = a + b \log N_{\text{HI}}$ , with  $a = 2.78$  and  $b = 0.93$ . The dotted lines show the  $\pm\sigma_{\text{int}}$  standard deviation of the relation, with  $\sigma_{\text{int}} = 1.27$ .  $N_{\text{HI}}$  was computed by assuming  $T_{\text{s}} = 100$  K and  $C_{\text{f}} = 1$ .

$\text{cm}^{-2}$ . Although both  $\sigma_{\text{int}}$  and the uncertainties on  $a$ ,  $b$ , and  $\sigma_{\text{int}}$  are large, the  $N_{\text{H}} - N_{\text{HI}}$  relation derived from the Bayesian analysis properly describes our data set, unlike the linear relations derived in Section 4.4. The results of the Bayesian analysis are displayed in Figure 3.

## 5 Conclusions

We performed spatially unresolved HI absorption observation of a sample of GPS/CSO galaxies with the WSRT, with the aim of improving the statistics of the  $N_{\text{H}} - N_{\text{HI}}$  correlation sample. We confirmed a significant, positive correlation between  $N_{\text{H}}$  and  $N_{\text{HI}}$ . For the full, censored data set, the generalized linear regression analysis yields  $N_{\text{H}} \propto N_{\text{HI}}^b$ , with  $b \simeq 0.6$ , although the goodness of this fit cannot be evaluated. For the detection subset, the linear regression analysis yields  $N_{\text{H}} \propto N_{\text{HI}}^b$ , with  $b \simeq 1$ , however the  $\chi^2$  is large. This fact may indicate that the  $N_{\text{H}} - N_{\text{HI}}$  relation is not a one-to-one relation: additional variables are involved in the correlation and generate the intrinsic spread of the data set. The Bayesian analysis applied to the detection subset enabled us to simultaneously quantify (i) the parameters of the  $N_{\text{H}} - N_{\text{HI}}$  relation, whose slope is  $b = 0.93^{+0.49}_{-0.33}$ , and (ii) the intrinsic spread on  $N_{\text{H}}$ ,  $\sigma_{\text{int}} = 1.27^{+1.30}_{-0.40}$ . The  $N_{\text{H}} - N_{\text{HI}}$  correlation suggests a connection between the intrinsic properties of the X-ray and HI absorbers. We are currently investigating the implications of this correlation, and we are attempting to identify and constrain the additional variables responsible for the intrinsic spread.

**Acknowledgements.** We thank the organisers of the Fifth Workshop on CSS and GPS sources for an extremely stimulating and enjoyable meeting. The research leading to these results has received

funding from the European Commission Seventh Framework Programme (FP/2007-2013) under grant agreement No 283393 (RadioNet3). L.O. acknowledges support from the ‘‘Helena Kluyver’’ programme run by ASTRON/JIVE, the INFN grant INDARK, the grant PRIN 2012 ‘‘Fisica Astroparticellare Teorica’’ of the Italian Ministry of University and Research, and the ‘‘Strategic Research Grant: Origin and Detection of Galactic and Extragalactic Cosmic Rays’’ funded by the University of Torino and Compagnia di San Paolo. L.O. is grateful to the Department of Physics and Astronomy of the University of Pennsylvania and to the High Energy Astrophysics Division of the Harvard-Smithsonian Center for Astrophysics for their support and kind hospitality. L.S. was supported by the Polish National Science Centre through the grant DEC-2012/04/A/ST9/00083. We are grateful to G.Józsa for his support during the observing runs with the WSRT and for providing us with the data-cubes of our target sources. We thank J.Buchner and M.Gruberbauer for developing their superb code APEMoST and making it available to the community. S.Andreon is acknowledged for a very stimulating seminar on Bayesian statistics. The WSRT is operated by ASTRON (Netherlands Institute for Radio Astronomy) with support from the Netherlands Foundation for Scientific Research (NWO).

## References

- Andreon, S., Hurn, M.A.: 2010, MNRAS 404, 1922
- Araya, E.D., Rodríguez, C., Pihlström, Y., Taylor, G.B., Tremblay, S., Vermeulen, R.C.: 2010, AJ 139, 17
- Carilli, C.L., Menten, K.M., Reid, M.J., Rupen, M.P., Yun, M.S.: 1998, ApJ 494, 175 [4]
- Curran, S.J., Allison, J.R., Glowacki, M., Whiting, M.T., Sadler, E.M.: 2013, MNRAS 431, 3408
- Guainazzi, M., Siemiginowska, A., Rodriguez-Pascual, P., Stanghellini, C.: 2004, A&A 421, 461 [13]
- Guainazzi, M., Siemiginowska, A., Stanghellini, C., Grandi, P., Piconcelli, E., Azubike Ugwoke, C.: 2006, A&A 446, 87 [9]
- Gruberbauer, M., Kallinger, T., Weiss, W.W., Guenther, D.B.: 2009, A&A 506, 1043
- Gupta, N., Salter, C.J., Saikia, D.J., Ghosh, T., Jeyakumar, S.: 2006, MNRAS 373, 972 [2]
- Isobe, T., Feigelson, E.D., Nelson, P.I.: 1986, ApJ 306, 490
- La Valley, M.P., Isobe, T., Feigelson, E.D.: 1992, BAAS 24, 839
- Migliori, G.: 2015, this Volume
- Mirabel, I.F., Sanders, D.B., Kazès, I.: 1989, ApJ 340, L9 [5]
- Morganti, R., Oosterloo, T.A., Tadhunter, C.N., Vermeulen, R., Pihlström, Y.M., van Moorsel, G., Wills, K.A.: 2004, A&A 424, 119
- Morganti, R., Fogasy, J., Paragi, Z., Oosterloo, T., Orienti, M.: 2013, Science 341, 1082
- Orienti, M.: 2015, this Volume
- Orienti, M., Morganti, R., Dallacasa, D.: 2006, A&A 457, 531 [1]
- O’Dea, C.P.: 1998, PASP 110, 493
- O’Dea, C.P., de Vries, W.H., Worrall, D.M., Baum, S., & Koekoer, A.: 2000, AJ 119, 478
- Ostorero, L., Moderski, R., Stawarz, Ł., Begelman, M.C., Diaferio, A., Kowalska, I., Kataoka, J., Wagner, S.J.: 2009, AN 330, 275
- Ostorero, L., Moderski, R., Stawarz, et al.: 2010, ApJ 715, 1071 [11]
- Peck, A.B., Taylor, G.B., Conway, J.E.: 1999, ApJ 521, 103 [8]
- Pihlström, Y.M., Conway, J.E., Vermeulen, R.C.: 2003, A&A 404, 871 [7]

- Press, W.H., Teukolsky, S.A., Vetterling, W.T., Flannery, B.P.: 1992, *Numerical recipes in FORTRAN. The art of scientific computing* (2nd ed.; Cambridge: Cambridge Univ. Press)
- Risaliti, G., Woltjer, L., Salvati, M.: 2003, *A&A* 401, 895 [14]
- Siemiginowska, A., La Massa, S., Aldcroft, T., Bechtold, J., Elvis, M.: 2008, *ApJ* 684, 811 [12]
- Siemiginowska, A.: 2009, *AN* 330, 264
- Snellen, I.A.G., Schilizzi, R.T., de Bruyn, A.G., Miley, G.K., Rengelink, R.B., Roettgering, H.J., Bremer, M.N.: 1998, *A&AS* 131, 435
- Stanghellini, C., O’Dea, C.P., Dallacasa, D., Baum, S.A., Fanti, R., Fanti, C.: 1998, *A&AS* 131, 303
- Tengstrand, O., Guainazzi, M., Siemiginowska, A., Fonseca Bonilla, N., Labiano, A., Worrall, D.M., Grandi, P., Piconcelli, E.: 2009, *A&A* 501, 89 [10]
- Torniainen, I., Tornikoski, M., Lähteenmäki, A., Aller, M.F., Aller, H.D., Mingaliev, M.G.: 2007, *A&A* 469, 451
- Vermeulen, R.C., Pihlström, Y. M., Tschager, W., et al.: 2003, *A&A* 404, 861 [3]
- Véron-Cetty, M.-P., Woltjer, L., Staveley-Smith, L., Ekers, R.D.: 2000, *A&A* 362, 426 [6]
- Vink, J., Snellen, I., Mack, K.-H., Schilizzi, R.: 2006, *MNRAS* 367, 928
- Wolfe, A.M. Burbidge, G.R.: 1975, *ApJ* 200, 548